

# Optical and transient photoconductive properties of pentacene and functionalized pentacene thin films: Dependence on film morphology

Oksana Ostroverkhova,<sup>a)</sup> Svitlana Shcherbyna, David G. Cooke, Ray F. Egerton, and Frank A. Hegmann<sup>b)</sup>

*Department of Physics, University of Alberta, Edmonton, Alberta T6G 2J1, Canada*

Rik R. Tykwinski

*Department of Chemistry, University of Alberta, Edmonton, Alberta T6G 2G2, Canada*

Sean R. Parkin and John E. Anthony

*Department of Chemistry, University of Kentucky, Lexington, Kentucky 40506-0055*

(Received 21 February 2005; accepted 19 May 2005; published online 3 August 2005)

We present a comprehensive study of the optical and transient photoconductive properties of pentacene and functionalized pentacene thin films grown by evaporation or from solution onto a variety of substrates. The transient photoconductivity was studied over picosecond time scales using time-resolved terahertz pulse spectroscopy. The structure and morphology of the films were assessed using x-ray diffraction, atomic force microscopy, and scanning electron microscopy. Regular pentacene films grown by evaporation under similar conditions but on different substrates yielded polycrystalline films with similar morphology and similar optical and transient photoconductive properties. Single exponential or biexponential decay dynamics was observed in all of the regular pentacene films studied. Functionalized pentacene films grown by evaporation at two different substrate temperatures (as well as from solution) yielded significant variations in morphology, resulting in different optical-absorption spectra and transient photoconductivities that could be correlated with film structure. The lower limit of the charge-carrier mobility, estimated from the amplitude of the transient photoconductive response, was  $\sim 0.02\text{--}0.04\text{ cm}^2/\text{V s}$  in the case of regular pentacene films and  $\sim 0.01\text{--}0.06\text{ cm}^2/\text{V s}$  in the case of functionalized pentacene films, depending on the film morphology. The best functionalized pentacene films exhibited transient photoconductivity values reaching  $\sim 30\%\text{--}40\%$  of those obtained in functionalized pentacene single-crystal samples, and showed similar power-law decay dynamics. We also report on terahertz pulse generation from voltage-biased pentacene thin films. © 2005 American Institute of Physics. [DOI: 10.1063/1.1949711]

## I. INTRODUCTION

For over 50 years, organic semiconductors have been investigated as an alternative to inorganic semiconductors in an effort to achieve low cost, easy fabrication, and tunable properties.<sup>1,2</sup> Applications envisioned for organic semiconductors include xerography, thin-film transistors, light-emitting diodes, solar cells, and many others.<sup>3,4</sup> Since most of these applications rely on the conductive and photoconductive properties of the materials, it is important to understand the physical mechanisms of charge photogeneration, transport, trapping, and recombination. However, despite numerous theoretical and experimental studies of the optical and electronic properties of organic solids, these mechanisms are not well understood and are still the subject of debate in the literature.<sup>5–7</sup> Indeed, it is a complicated task to reveal the *intrinsic* properties of organic materials, since they are often masked by the influence of impurities, the presence of which is very sensitive to the methods of material purification and device fabrication.<sup>8–11</sup> In addition, most experimental tech-

niques that assess the electronic properties of materials require the application of static electric fields with deposited electrodes. The processes occurring at the metal-organic interfaces at the electrodes can significantly affect the performance of a device,<sup>12</sup> making it difficult to observe the intrinsic properties of the material.

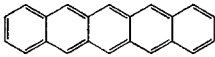
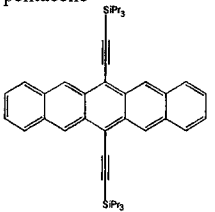
Since many applications proposed for organic semiconductors would utilize thin-film geometries, it is necessary to understand the relationships between morphology and the optical and charge transport properties of the films. This, in turn, could help improve the film preparation methods. It is well known that optical-absorption spectra and charge-carrier mobilities of organic films are sensitive to the film structure and morphology.<sup>10,11,13–20</sup> Often, however, structure-property relationships are not straightforward<sup>9,10,20</sup> and, therefore, comprehensive studies that simultaneously link a variety of properties to film morphology are in demand.<sup>11,18</sup>

Time-resolved terahertz pulse spectroscopy is an experimental technique that uses electromagnetic pulses in the terahertz part of the spectrum to explore the far-infrared conductivity and ultrafast carrier dynamics in various classes of materials.<sup>21,22</sup> Optical-pump-terahertz-probe time-resolved spectroscopy allows the transient photoconductive properties of materials to be measured with subpicosecond time resolu-

<sup>a)</sup>Permanent address: Department of Physics, Oregon State University, Corvallis, Oregon 97331.

<sup>b)</sup>Electronic mail: hegmann@phys.ualberta.ca

TABLE I. Summary of thin-film and single-crystal samples used in our study.

Material	Sample	Preparation method	Substrate	Substrate temperature $T_s$ (°C)	Thickness ( $\mu\text{m}$ )
 Pentacene	Pc 1 and 1'	evaporation	mica	25	0.25
	Pc 2	evaporation	KCl	25	0.3
	Pc 3 and 3'	evaporation	mica	25	0.15
	Pc 4	evaporation	glass	25	0.25
 TIPS-functionalized pentacene	FPC 1a, 1a', and 1b	evaporation	mica glass	25	0.52
	FPC 2a and 2b	evaporation	mica glass	85	0.8
	FPC 3a and 3b	evaporation	mica glass	25	0.33
	FPC 4	solution	glass	25	1.3
	FPC	solution	...	...	300–500
	crystals				

tion, and has the added advantage of being a *non contact* technique (i.e., no electrodes required). In this technique, the transmission of a terahertz pulse through a sample in the presence of optical excitation is measured as a function of the delay time between the optical-pump and the terahertz probe pulses. Optical-pump–terahertz-probe spectroscopy has been utilized in studies of nonequilibrium carrier dynamics in a variety of materials such as inorganic semiconductors,<sup>23,24</sup> semiconductor nanoparticles,<sup>25</sup> liquids,<sup>26</sup> insulators,<sup>27</sup> organic crystals,<sup>28,29</sup> and has recently been extended to polymers<sup>30</sup> and polyacene thin films.<sup>31</sup> It is a valuable technique for probing the photogeneration of mobile charge carriers, intrinsic charge transport, and structure-property relationships. Recently, optical-pump–terahertz-probe spectroscopy allowed us to observe subpicosecond charge-carrier photogeneration and bandlike charge transport in functionalized pentacene single crystals as well as regular and functionalized pentacene thin films.<sup>28,31,32</sup>

In this article, we report on the optical properties and ultrafast carrier dynamics in a variety of pentacene and functionalized pentacene thin films. We correlate the optical-absorption spectra and transient photoconductivity of the films with their morphology, as studied by atomic force and scanning electron microscopies. The paper is organized as follows: Sec. II describes the materials studied, the sample preparation methods, and the experimental procedures used in characterization of the morphological, optical, and transient photoconductive properties of the samples. Section III presents the results from x-ray diffraction, atomic force and/or scanning electron microscopy, optical-absorption spectra, and transient photoconductive properties of pentacene (Sec. III A) and functionalized pentacene (Sec. III B) samples. Section IV discusses the results in the context of structure-property relationships, and a summary is given in Sec. V.

## II. EXPERIMENT

### A. Materials

In our studies, we used thin films of regular pentacene (Pc) and a pentacene derivative functionalized with the tri-

isopropylsilylethynyl (TIPS) side groups (FPC).<sup>33,34</sup> Pc was obtained from Aldrich and used without further purification. All of the Pc and most of the FPC films were prepared on mica, glass, or KCl substrates by thermal evaporation of the corresponding powder heated to 200–250 °C in high vacuum ( $10^{-6}$ – $10^{-7}$  Torr) at a deposition rate of 0.3 Å/s. Chemical structures of the molecules as well as information about the films discussed in this paper are given in Table I, where different samples prepared simultaneously (i.e., under exactly the same deposition conditions) on the same type of substrate are presented as, for example, Pc 1 and 1', whereas those prepared simultaneously but on different substrates are labeled as, for example, FPC 2a and 2b. During the vacuum deposition of all Pc films (Pc 1–4) and FPC films 1 (FPC 1a, 1a', and 1b) and 3 (FPC 3a, 3a', and 3b), the substrate was maintained at room temperature ( $T_s=25$  °C), while the films FPC 2 (FPC 2a and 2b) were obtained at a substrate temperature of  $T_s=85$  °C. The film FPC 4 was cast from tetrahydrofuran (THF) solution on a glass substrate at room temperature. Compared to the FPC films thermally evaporated at  $T_s=25$  °C, those grown from a solution or thermally evaporated at elevated substrate temperature yielded larger crystalline domains and exhibited improved photoconductive properties, as we discuss later in the paper. The thickness of the films was measured with a profilometer (Tencor Instruments) and ranged between 150 nm and 1.3  $\mu\text{m}$  (Table I). FPC single-crystal samples were grown from solution and typically had dimensions of  $2\times 4$  mm<sup>2</sup> and a thickness of 0.3–0.5 mm.<sup>28,33,35</sup>

It is well known that polycyclic aromatic hydrocarbons including pentacene and its derivatives can be unstable in the presence of light and oxygen.<sup>36,37</sup> Although we did not observe any photobleaching and/or degradation in the Pc films, some FPC films showed signs of partial photobleaching under ambient light within several months. Therefore, all the measurements reported here were carried out using freshly prepared samples that were stored in the dark between experiments, so that no day-to-day variation in the optical and photoconductive properties of the samples was observed. Furthermore, many FPC thin films slowly degraded under

pulsed laser illumination, with the transient photoconductivity signals reduced by 20% after  $\sim 15$ – $30$  min of pulsed illumination at 580 nm, for the laser fluences typically used in our experiments (Sec. II D). In order to avoid this problem, pulsed illumination of the same spot on a FPc film was limited to  $\sim 2$ – $10$  min, depending on the film, after which the sample was translated to a new region.

Interestingly, more-crystalline FPc films exhibited much slower photodegradation than the amorphous ones, and for the FPc 4 thin film and the FPc single-crystal samples, we did not observe any photodegradation of the photoresponse even after many hours of pulsed illumination. In addition, all the FPc crystals, the FPc 4 film, and all of the Pc films were very stable with respect to photo-oxidation in air under ambient light and have not shown any signs of degradation over a period of at least one year. All the Pc and FPc samples studied exhibited the same values of photoconductivity when exposed to air or kept in vacuum.

## B. Optical absorption

For measurements of the optical-absorption spectra of the films, the light from a tungsten source was coupled to a fiber for illumination at normal incidence. The light transmitted through the samples was collected by a second fiber and analyzed using a charge-coupled device (CCD) spectrometer (Ocean Optics). All spectra obtained from the thin-film samples were referenced to those of the corresponding substrates, whereas the spectra from solutions were referenced to those of the solvents. For measurements of temperature dependence, the thin-film samples were mounted on 1.5-mm apertures and placed in an optical cryostat (sample in vapor). The measurements were carried out in the range of 10–290 K, both in cooling and heating modes. The changes in the absorption spectra of all our samples with the temperature were gradual, completely reversible, and did not depend on the thermal cycling of the sample. The data were taken at 30–40-K intervals, and at each temperature they were referenced with respect to the corresponding substrate.

## C. Characterization of film structure and surface morphology

Glancing angle x-ray diffraction was performed on the films using a CCD diffractometer (Bruker-Nonius X8 Proteum) with a rotating copper anode and graded-multilayer focusing optics. The angle between the plane of the sample and the incident beam was  $4^\circ$ , and the sample-to-detector distance was 100 mm. During exposure, the sample was rotated a full  $360^\circ$  about the normal to the film surface. Atomic force microscopy (AFM) images were obtained at room temperature using a multimode AFM (Digital Instruments) in tapping mode with Si cantilevers oscillating at a frequency of 100–300 kHz. The lateral resolution was about 15 nm. Secondary electron micrographs were obtained at room temperature using a Hitachi S-4800 (cold tip field emission) scanning electron microscope (SEM). No conductive coating was applied to the sample surface. The electron beam was at normal incidence to the sample, and the accelerating voltage was 1.5–3 kV.

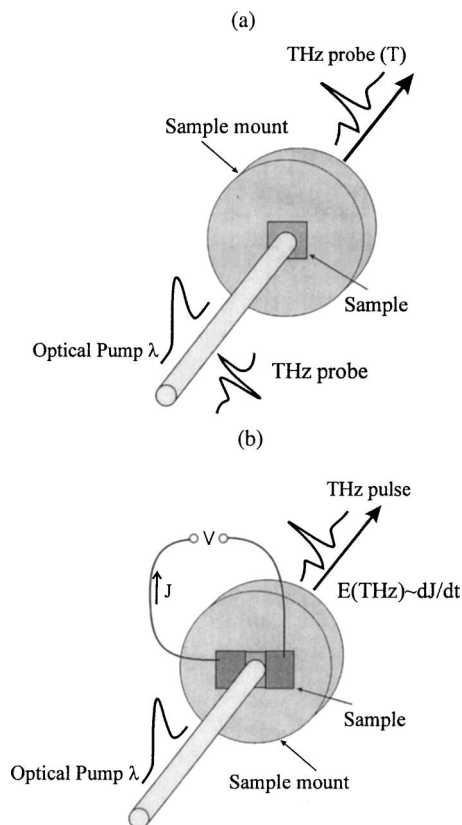


FIG. 1. Schematic for (a) optical-pump-terahertz probe experiments and (b) terahertz generation experiments.

## D. Transient photoconductivity

### 1. Optical-pump-terahertz-probe experiments

A detailed description of the optical-pump-terahertz-probe experimental setup has been reported elsewhere.<sup>24,38</sup> Briefly, an amplified Ti:sapphire laser source (800 nm, 100 fs, 1 kHz) was used to produce optical-pump pulses at a wavelength of  $\lambda \sim 580$  nm through optical parametric amplification and terahertz probe pulses generated via optical rectification in a 0.5-mm-thick ZnTe crystal. The samples were mounted on 1–2-mm apertures, and both the terahertz-probe and optical-pump pulses were at normal incidence to the surface of the films or  $a$ - $b$  plane of the single-crystal samples [Fig. 1(a)]. The experiments were carried out in air at room temperature. The electric field of the terahertz pulse transmitted through the samples,  $T(t)$ , was detected by free-space electro-optic sampling in a 2-mm-thick ZnTe crystal and monitored at various delay times ( $\Delta t$ ) with respect to the optical-pump pulse. Terahertz transmissions through the substrates used in our experiments were 88%, 44%, and 30% in the cases of mica, KCl, and glass substrates, respectively; among the films grown on different substrates under the same conditions, the best signal-to-noise ratio in photoconductivity transients was obtained in films grown on mica, due to its relative transparency at terahertz frequencies. The range of optical-pump fluences employed in our experiments was 0.9–1.5 mJ/cm<sup>2</sup>. No transient photoconductivity was observed upon optical excitation of the substrates alone. Optical excitation of all thin-film and single-crystal samples

with  $\lambda \sim 580$  nm resulted in a change in the transmitted electric field  $[-\Delta T(t)]$  due to the transient photoconductivity (i.e., *mobile* photocarriers).<sup>31</sup> We note that the polarization of photogenerated neutral excitons by the terahertz electric field would result in a phase shift between the  $-\Delta T(t)$  and  $T(t)$  wave forms.<sup>39</sup> However, in the absence of this phase shift, as was the case for all our samples, the optically induced relative change in the terahertz peak amplitude  $[-(T-T_0)/T_0 \equiv -\Delta T/T_0]$ , where  $T_0$  is the amplitude of the terahertz pulse transmitted through unexcited sample] provides a direct measure of the transient photoconductivity.<sup>28,29,31</sup> In the approximation of a thin conducting film on an insulating substrate, the differential transmission  $(-\Delta T/T_0)$  due to optical excitation of mobile carriers at small  $|\Delta T/T_0|$  is related to the transient photoconductivity as follows:<sup>24,28,29</sup>  $\sigma = -(\Delta T/T_0)(1 + N)/(Z_0 d)$ , where  $Z_0 = 377 \Omega$  is the impedance of free space,  $N$  is the refractive index of the substrate at terahertz frequencies, and  $d$  is the film thickness. Using this expression, and setting the maximum value for the transient response at  $\Delta t = 0$  so that  $|\Delta T/T_0|_{\max} = |\Delta T(0)/T_0|$ , the product of the charge-carrier mobility ( $\mu$ ) and photogeneration efficiency ( $\eta$ ) can be calculated as follows:<sup>31</sup>

$$\mu\eta = \left| \frac{\Delta T(0)}{T_0} \right| \frac{h\nu(1+N)}{eF(1-R)(1 - \exp[-\alpha d])Z_0}, \quad (1)$$

where  $e$  is the electric charge,  $h$  is Planck's constant,  $\nu$  is the light frequency,  $\alpha$  is the absorption coefficient,  $F$  is the incident fluence, and  $R$  is the reflection coefficient.

## 2. Terahertz generation experiments

Gold (Au) electrodes 110 nm thick were deposited on some of the Pc thin-film samples by thermal evaporation through a shadow mask, leaving a gap of  $330 \mu\text{m}$  between the electrodes. These samples were mounted on an aperture and optically excited with 580-nm, 100-fs pulses at a fluence of  $\sim 0.7 \text{ mJ/cm}^2$  at normal incidence [Fig. 1(b)]. The bias voltage ( $V$ ) was applied using a dc high-voltage power supply. The electric field of the terahertz pulse,  $E(\text{THz})$ , emitted from the sample was detected by free-space electro-optic sampling in a 2-mm-thick ZnTe crystal.<sup>24,38</sup>

## III. RESULTS

### A. Pentacene

#### 1. Morphology and optical properties

Pc films prepared as described in Sec. II A yielded polycrystalline structures. X-ray-diffraction analysis revealed that the crystallites in all Pc films (Pc 1–4) were oriented with their  $c$  axis perpendicular to the substrate, in agreement with previous studies of similarly prepared films.<sup>4,40</sup> AFM confirmed a dendritic grain structure that appears to be characteristic of polycrystalline pentacene films.<sup>10,40,41</sup> The average grain size was approximately  $0.7\text{--}1.2 \mu\text{m}$  (e.g.,  $\sim 1\text{--}1.2 \mu\text{m}$  in the film Pc 4, as shown in Fig. 2). The grain size was slightly dependent on the substrate, with the largest average grain size obtained in films deposited on a glass substrate.<sup>32</sup>

Optical-absorption spectra of our polycrystalline Pc films did not vary appreciably from film to film and were

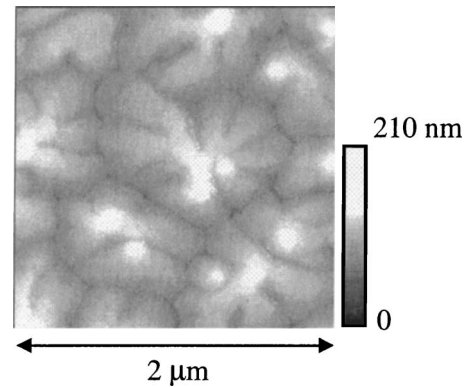


FIG. 2. Atomic force microscopy image of the film Pc 4 (on glass). The dimensions of the image are  $2 \times 2 \mu\text{m}^2$ , and the vertical scale is 210 nm.

similar to those reported in the literature.<sup>2,6,13,14,17,42,43</sup> It is characteristic for aromatic-type organic materials to exhibit a redshift (or displacement  $\Delta$ ) of the absorption spectrum in the solid phase compared to the gas phase or in a nonpolar solution due to enhanced Coulomb interaction of the molecule with its surrounding and exchange interactions between translationally equivalent molecules.<sup>2,44</sup> The displacement ( $\Delta$ ) is different for each electronic state; it depends on the transition moments and molecular-orbital overlap; and if the spectrum of the solid phase is compared with that of a solution,  $\Delta$  depends on the polarity of the solvent. In the case of the lowest electronic transition, the displacement can exhibit values as low as  $\sim 10 \text{ cm}^{-1}$  (as for benzene single crystals compared to a benzene solution in ethanol<sup>44</sup>) and as high as  $\sim 2500 \text{ cm}^{-1}$ , depending on the material (e.g.,  $\Delta \sim 1000\text{--}1500 \text{ cm}^{-1}$  in anthracene and tetracene single crystals compared to their respective solutions in ethanol<sup>44</sup> and  $\Delta \sim 2400 \text{ cm}^{-1}$  in polycrystalline pentacene films compared to solutions of pentacene in benzene<sup>13</sup>). As seen from Fig. 3(a), in our Pc films, the displacement of  $\sim 95 \text{ nm}$  ( $\sim 2400 \text{ cm}^{-1}$ ) with respect to the spectrum of Pc solution in chlorobenzene ( $\text{C}_6\text{H}_5\text{Cl}$ ) is obtained, similar to that in Ref. 13. In addition, Davydov splitting<sup>45</sup> due to interaction of translationally nonequivalent molecules, characteristic of crystals with several molecules per unit cell (two in the case of Pc),<sup>2</sup> is clearly observed in the spectra of the Pc films [e.g.,  $a$  and  $b$  bands in the spectrum of the film Pc 4 in Fig. 3(a)]. From the literature, the values for Davydov splitting of the 0-0 band obtained in Pc samples range from  $\sim 880 \text{ cm}^{-1}$  in the case of quasicrystalline films<sup>14</sup> to  $1100 \text{ cm}^{-1}$  in the case of single crystals. Also, the values of  $\sim 900$  and  $990 \text{ cm}^{-1}$  have been reported in Pc films in the “thin-film phase” and “single-crystalline phase,” respectively.<sup>42</sup> In our Pc films, Davydov splitting values of  $\sim 960\text{--}1050 \text{ cm}^{-1}$  were obtained at room temperature, depending on the film, which suggests the prevalence of the single-crystalline phase in all samples.

Figure 3(b) shows an absorption spectrum of the film Pc 4 as a function of temperature (for clarity, only the data at 290, 200, and 10 K are shown). As the temperature decreases, several gradual changes occur in the spectrum. First of all, the absorption tail observed from 720 to 780 nm at 290 K, which is likely due to transitions originating at higher

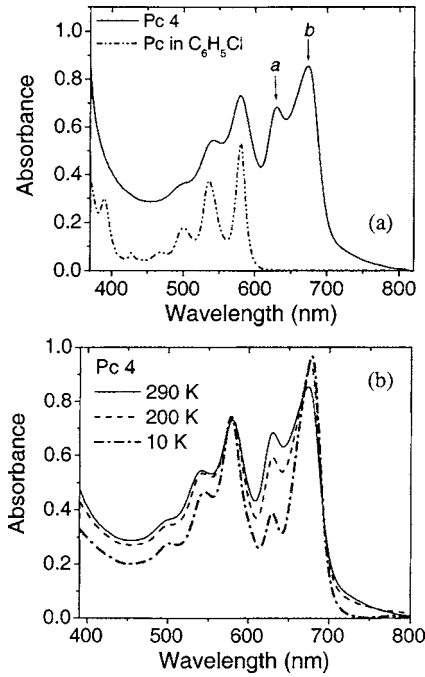


FIG. 3. (a) Optical-absorption spectra of the film Pc 4 (solid line) and a dilute solution of Pc in chlorobenzene  $C_6H_5Cl$  (dash-dotted line) at room temperature. The *a* and *b* bands of the 0-0 Davydov doublet are indicated. (b) Optical-absorption spectrum of the film Pc 4 at 290 K (solid line), 200 K (dashed line), and 10 K (dash-dotted line).

vibronic levels of the ground state,<sup>44</sup> becomes less pronounced at lower temperatures and completely disappears at 10 K. We note that absorption tails in polyacenes have also been attributed to defect states and disorder.<sup>14,46</sup> Second, at low temperatures the absorption bands are better resolved, which could be due to reduction in lifetime broadening effects.<sup>2</sup> In addition, the Davydov splitting increases by  $\sim 150\text{ cm}^{-1}$  upon cooling from 290 to 10 K, indicative of enhanced intermolecular interaction.<sup>17</sup> Finally, the relative strength of various bands, including the *a* and *b* transitions (Fig. 3), changes with the temperature, which has been previously observed in tetracene and pentacene thin films and attributed to molecular reorientations that cause changes in mutual molecular overlap within the unit cell.<sup>14,15,47</sup>

## 2. Transient photoconductive properties

*a. Optical-pump-terahertz-probe experiments.* As we discussed in Sec. III A 1, in all our Pc films, the crystallites are oriented with their *c* axis perpendicular to the substrate. Therefore, the electric field of the terahertz pulse probes the transient photoconductivity in the *a-b* plane of the crystallites. Figure 4 shows the negative differential transmission ( $-\Delta T/T_0$ ) of the terahertz-probe pulse as a function of delay time ( $\Delta t$ ) between the optical-pump and terahertz-probe pulses, which reflects the dynamics of the transient photoconductivity (Sec. II D) in thin films Pc 1, Pc 3, and Pc 4. The transient photoconductivity observed in all Pc films is characterized by fast charge photogeneration that occurs in a time less than 400 fs,<sup>31</sup> limited by the time resolution of our setup, followed by decay due to carrier trapping and recombination. The product of charge-carrier mobility ( $\mu$ ) and photogeneration efficiency ( $\eta$ ) calculated from Eq. (1) using the

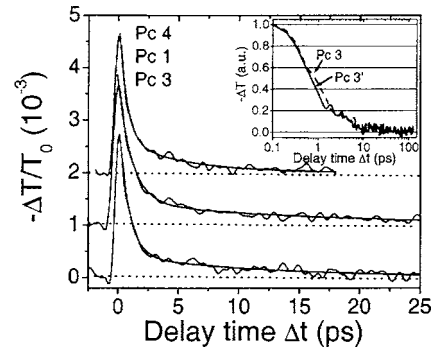


FIG. 4. Differential transmission ( $-\Delta T/T_0$ ) as a function of pump-probe delay time ( $\Delta t$ ) obtained in Pc 1, 3 (both on mica), and 4 (on glass) thin films under optical excitation at  $\lambda \sim 580\text{ nm}$  in air at room temperature. Fits with a biexponential function are also shown (parameters are listed in Table II). The transients are offset along the y axis for clarity. The inset shows the  $-\Delta T$  transients normalized to their values at  $\Delta t=0$  obtained under the same conditions in the Pc 3 and Pc 3' films (both on mica).

maximum amplitude  $|\Delta T(0)/T_0|$  of the transient response exhibited similar values of  $\sim 0.02\text{--}0.04\text{ cm}^2/\text{V s}$  in all the Pc films studied (Table II) and did not reflect small differences in the grain size of the films grown on different substrates.<sup>32</sup> Moreover, in all of the Pc films the decay dynamics at room temperature could be described either by a single exponential ( $\propto \exp[-\Delta t/\tau]$ ) with a time constant  $\tau \sim 0.7\text{--}1\text{ ps}$  (Refs. 31 and 32) or biexponential ( $\propto A \exp[-\Delta t/\tau_1] + B \exp[-\Delta t/\tau_2]$ ) with the contribution of the fast decay component ( $\tau_1 \sim 0.6\text{--}1.2\text{ ps}$ ) dominating over that of the slow decay component ( $\tau_2 \sim 5\text{--}16\text{ ps}$ ) with  $A/(A+B) > 0.75$ , depending on the sample (Table II). Although it is not straightforward to relate the charge-carrier mobility to the grain size of the polycrystalline films,<sup>10</sup> longer decays of the transient photoconductivity due to fewer grain boundaries that serve as trapping sites would be expected in films with a larger grain size. However, although the grain size ( $\sim 1\text{--}1.2\text{ }\mu\text{m}$ ) in our Pc films grown on a glass substrate was slightly larger than in those grown on mica ( $0.7\text{--}0.8\text{ }\mu\text{m}$ ), this difference did not result in significantly different decay dynamics (Fig. 4). As seen from the parameters of the fits (Table II), the sample-to-sample variation in our signals is not due to the substrate-related difference in morphology, since similar differences in the decay dynamics were obtained in films grown on the same substrate (e.g., Pc 1 and Pc 3'). Moreover, some differences in the decay dynamics were observed even in films grown on the same substrate under identical conditions (e.g., Pc 1 and Pc 1'), which suggests that local defects may influence the transients. As a result, even in our best Pc films, the deep-level trapping on grain boundaries, defects, and/or chemical impurities prevented the observation of the carrier transport on time scales above  $\sim 20\text{--}30\text{ ps}$  after photoexcitation (inset of Fig. 4).

*b. Terahertz generation experiments.* One of the manifestations of ultrafast carrier generation and high charge-carrier mobility in our Pc films is terahertz generation due to acceleration of the photogenerated carriers by an applied static electric field in a voltage-biased sample.<sup>22</sup> While ultrafast photoconductive switches that produce terahertz generation have been studied extensively in inorganic materials,<sup>48</sup> most

TABLE II. Summary of transient photoconductivity results.

Sample	Decay dynamics	$\beta^a$	$\tau_1$ (ps) <sup>b</sup>	$\tau_2$ (ps) <sup>b</sup>	$A/(A+B)^b$	$\frac{\mu\eta}{\text{cm}^2/(\text{V s})}^c$
Pc 1	Bi exp	...	1.14	16	0.83	0.03
1'	Single exp	...	0.97	...	1	0.02
Pc 2	Single exp	...	0.71	...	1	0.03
Pc 3	Bi exp	...	0.82	12	0.86	0.04
3'	Bi exp	...	0.72	9.3	0.92	0.03
Pc 4	Bi exp	...	0.64	5	0.79	0.03
FPc 1	...	...	...	...	...	$\leq 0.01$
FPc 2	Power law	0.53	...	...	...	0.06
FPc 3a	Single exp	...	1.35	...	1	0.03
3a'	Single exp	...	0.64	...	1	0.025
FPc 4	Power law	0.53	...	...	...	0.06
FPc single crystals	Power law	0.5–0.7	...	...	...	0.15–0.2

<sup>a</sup>Power-law exponent ( $\beta$ ) obtained by fitting the differential transmission  $[-\Delta T(\Delta t)/T_0]$  as a power-law function  $(\Delta t^{-\beta})$  of the optical-pump–terahertz-probe delay time ( $\Delta t$ ).

<sup>b</sup>Parameters obtained from a single exponential ( $\exp[-\Delta t/\tau_1]$ ) or biexponential ( $A \exp[-\Delta t/\tau_1] + B \exp[-\Delta t/\tau_2]$ ) fit to the decay dynamics.

<sup>c</sup>The product of mobility ( $\mu$ ) and photogeneration efficiency ( $\eta$ ) calculated from the peak of transient photoconductivity  $[-\Delta T(0)/T_0]$  using Eq. (1).

organic terahertz emitters utilize optical rectification in a noncentrosymmetric crystal or poled polymer to produce terahertz generation.<sup>49</sup> To date, the only reports of terahertz generation from organic semiconductor photoconductive switches have been based on poly(phenylene vinylene) (PPV) polymer films.<sup>50</sup> Figure 5 shows the terahertz pulse generated in the film Pc 2 upon optical excitation at the wavelength of  $\sim 580$  nm at a voltage bias of 700 V (solid line), which corresponds to an applied electric field of  $\sim 21$  kV/cm. The polarity of the terahertz pulse depended on that of the applied voltage, and no signal was detected at zero bias (Fig. 5, dashed line), which confirms that the observed terahertz generation is not due to any possible optical rectification effects.<sup>49</sup> In general, the spectrum of the terahertz pulse generated in a biased photoconductor depends on the sample geometry, photoconductivity of the material, bias voltage, and the optical excitation density.<sup>21,51</sup> In our experimental geometry (Sec. II D) at an incident fluence of  $\sim 0.7$  mJ/cm<sup>2</sup> and an applied voltage of 700 V, the spectrum of the terahertz transient generated in the film Pc 2 is cen-

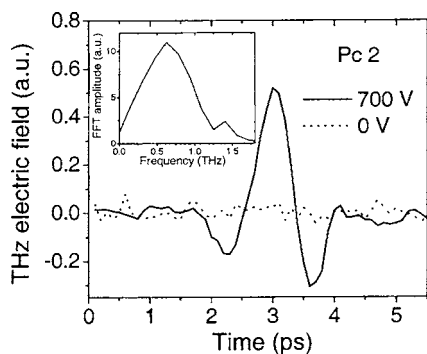


FIG. 5. Terahertz pulse generated (solid line) from the film Pc 2 (on KCl) upon optical excitation at  $\lambda \sim 580$  nm and a voltage bias of 700 V corresponding to an electric field of 21 kV/cm. No signal is observed at zero bias (dashed line). The inset shows the Fourier amplitude spectrum of the terahertz pulse.

tered at  $\sim 0.6$  THz and has a bandwidth of about 0.8 THz with frequency components up to  $\sim 1.7$  THz (inset of Fig. 5). This is comparable with the terahertz pulse spectra obtained from biased low-temperature (LT)-GaAs photoconductive switches,<sup>51</sup> and further shows that mobile photo carriers in pentacene are generated in subpicosecond time scales. Ultrafast photogeneration of mobile charge carriers within subpicosecond time scales was also reported in the terahertz emission experiments using voltage-biased PPV polymer thin films.<sup>50</sup>

## B. Functionalized pentacene

### 1. Morphology and optical properties

The structure and morphology of the FPc thin films were independent of the substrate used but sensitive to the preparation conditions and the film thickness. Figure 6(a) shows the absorption spectra of a dilute solution of FPc molecules in THF (dash-dotted line) and the film FPc 1b (solid line) at room temperature, similar to the spectra obtained in TIPS FPc samples in Refs. 52 and 37. The spectra of the films FPc 2b, FPc 3b, and FPc 4 are significantly different, as seen in Fig. 6(b) (dash-dotted, solid, and dashed lines, respectively, all at room temperature). In contrast with regular Pc molecules that form a “herringbone-type” packing structure in a crystal with two molecules per unit cell, the TIPS FPc molecules assume a “brick-wall-type” packing<sup>28,33</sup> with one molecule per unit cell and, therefore, no Davydov splitting is expected in the spectra of FPc films. As we discussed in Sec. III A 1, a redshift (or displacement  $\Delta$ ) of the absorption spectrum is expected in the solid phase compared to the gas phase or in solution, regardless of the number of molecules per unit cell. In our FPc films, the displacement  $\Delta$  of the lowest electronic transition depends on the structure and morphology of the films. For example, as seen from Fig. 6, the redshift of the spectrum of the film FPc 1 compared to that of FPc molecules in THF is only about 5 nm

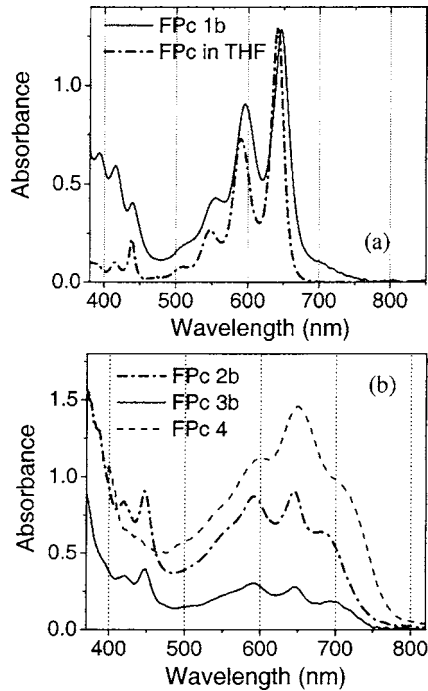


FIG. 6. Optical-absorption spectra of (a) FPC in THF solution (dash-dotted line) and FPC *1b* thin film (evaporated at  $T_s=25^\circ\text{C}$ , on glass) (solid line), and (b) FPC *2b* (evaporated at  $T_s=85^\circ\text{C}$ , on glass), *3b* (evaporated at  $T_s=25^\circ\text{C}$ , on glass), and *4* (solution grown at  $T_s=25^\circ\text{C}$ , on glass) films (dash-dotted, solid, and dashed lines, respectively).

( $\sim 220\text{ cm}^{-1}$ ), while in the films FPC *2b*, FPC *3b*, and FPC *4* it is much larger ( $\Delta \sim 45\text{--}70\text{ nm}$ , or  $1000\text{--}1500\text{ cm}^{-1}$ , depending on the film). In addition, the widths of the bands as well as the relative strengths of the vibronic transitions vary from film to film. In particular, broader bands (indicative of stronger intermolecular interaction)<sup>2</sup> and stronger coupling between electronic and vibronic modes<sup>2</sup> are observed in the films FPC *2b*, FPC *3b*, and FPC *4* compared to that in the FPC solution and the film FPC *1*. The similarity between the spectra of the FPC solution and the film FPC *1* indicates the prevalence of an amorphous phase in this film.<sup>14</sup> Indeed, for a random molecular distribution, the bulky TIPS side groups<sup>33</sup> prevent the  $\pi$  stacking, which weakens the features that are typically observed in the optical spectra of solid-state samples with a crystalline structure. Figure 7(a) shows the AFM image of the film FPC *1*, which reveals smooth featureless domains with sparse crystallites separated by  $1\text{--}2\ \mu\text{m}$ , the latter being responsible for the weak absorption band at  $\sim 680\text{--}750\text{ nm}$  observed in the absorption spectrum of the film [Fig. 6(a)]. In contrast with FPC *1*, the films FPC *2b*, FPC *3b*, and FPC *4* exhibit polycrystalline structures with significant crystalline coverage, as seen in the AFM image of the film FPC *2b* [Fig. 7(b)], that result in a large solid-state shift ( $\Delta$ ) and broader bands in the optical-absorption spectra as well as improved transient photoconductive properties (Sec. III B 2). The x-ray-diffraction analysis revealed that the crystallites in films FPC *2*–*4* were oriented predominantly with the  $c$  axis perpendicular to the substrate.

The temperature dependence of the absorption spectra of FPC thin films is drastically different from that of the regular Pc films (Fig. 3). Figures 8(a) and 8(b) show the absorption

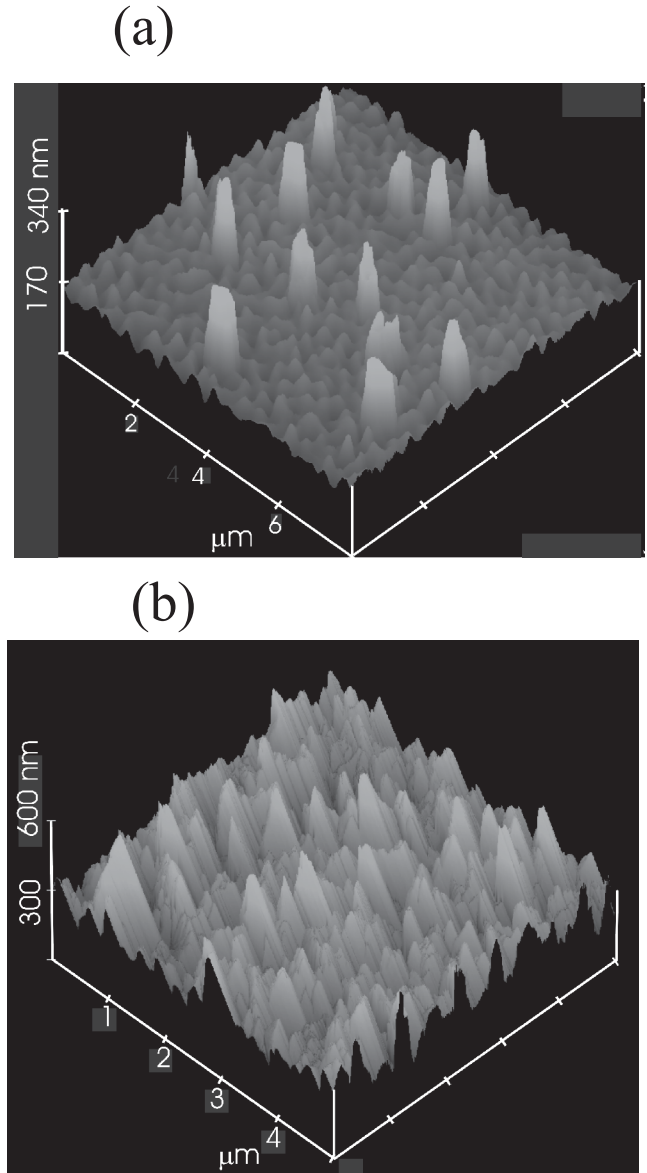


FIG. 7. Atomic force microscopy images of the films (a) FPC *1b* (evaporated at  $T_s=25^\circ\text{C}$ , on glass), and (b) FPC *2b* (evaporated at  $T_s=85^\circ\text{C}$ , on glass).

spectra of the films FPC *2b* and FPC *3b*, respectively, at 290, 200, and 10 K. As the temperature is lowered, the most pronounced feature of these spectra is the significant redshift of the lowest-energy absorption peak upon cooling from 290 to 200 K (centered at  $\sim 685$  and  $\sim 693\text{ nm}$  at 290 K and at  $\sim 692$  and  $\sim 704\text{ nm}$  at 200 K in the films FPC *2b* and *3b*, respectively), followed by its splitting into two bands upon further cooling to 10 K (centered at  $\sim 688$  and  $\sim 733\text{ nm}$  in the film FPC *2b* and at  $\sim 682$  and  $\sim 733\text{ nm}$  in the film FPC *3b*). Similar to Pc films, the change in the absorption spectrum of FPC films with the temperature was completely reversible and did not depend on the substrate (e.g., identical changes in the spectra of the films FPC *3a* and *3b* were observed as a function of temperature). A redshift of the absorption spectra upon cooling has been reported in conjugated polymers and attributed to increased conjugation and exciton delocalization due to freezing out of the torsional and other low-frequency vibrational modes that disrupt conjuga-

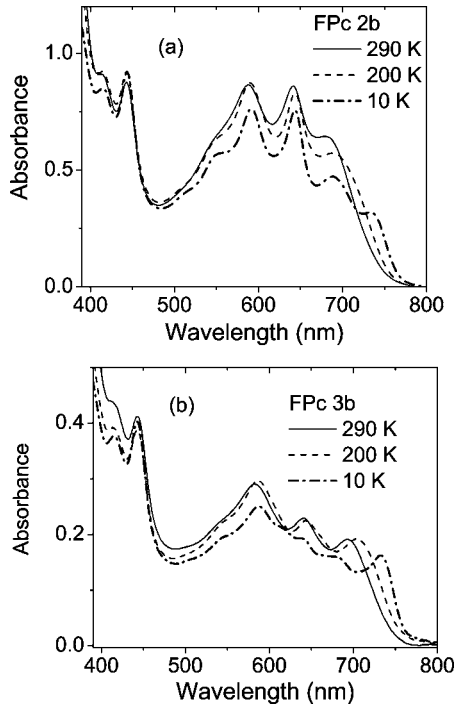


FIG. 8. Optical-absorption spectra of the films: (a) FPC 2*b* (evaporated at  $T_s=85^\circ\text{C}$ , on glass), and (b) FPC 3*b* (evaporated at  $T_s=25^\circ\text{C}$ , on glass) at 290 K (solid line), 200 K (dashed line), and 10 K (dash-dotted line).

tion and reduce the  $\pi$  and  $\pi^*$  bandwidths.<sup>53</sup> In our FPC films, a similar mechanism could be accountable for the temperature dependence of the absorption spectra, as low-frequency vibrational modes due to the bulky TIPS side groups in the FPC molecules freeze-out upon cooling, improving  $\pi$  stacking. Interestingly, no significant shift of the absorption edge as a function of temperature was observed in FPC single-crystal samples, at least at temperatures ranging between 65 and 298 K.<sup>35</sup>

## 2. Transient photoconductivity (optical-pump—terahertz-probe experiments)

The transient photoconductivity signals obtained in various FPC films using the optical-pump—terahertz-probe time-resolved technique (Sec. II D) were all characterized by a fast rise ( $<400$  fs, limited by the time resolution of our setup), but differed in amplitude and decay dynamics depending on the morphology of the film. The films prepared simultaneously (i.e., under identical conditions), but on different substrates (e.g., films FPC 3*a* and FPC 3*b*) yielded similar transients. Figure 9(a) illustrates the transient differential transmission ( $-\Delta T/T_0$ ) obtained in the films FPC 2*a*, FPC 3*a*, and FPC 4 at room temperature. Since in these films the crystallites are oriented with their  $c$  axis perpendicular to the substrate (as confirmed by the x-ray-diffraction analysis), the electric field of the terahertz pulses probes the transient photoconductivity in the  $a$ - $b$  plane of the crystallites, which has higher mobility than the transport along the  $c$  axis.<sup>33</sup> The product  $\mu\eta$  of charge-carrier mobility ( $\mu$ ) and photogeneration efficiency ( $\eta$ ) calculated from the amplitude of the transients using Eq. (1) yielded a value of about  $0.03\text{ cm}^2/\text{V s}$  in the films FPC 3*a* and FPC 3*b* (prepared by evaporation at

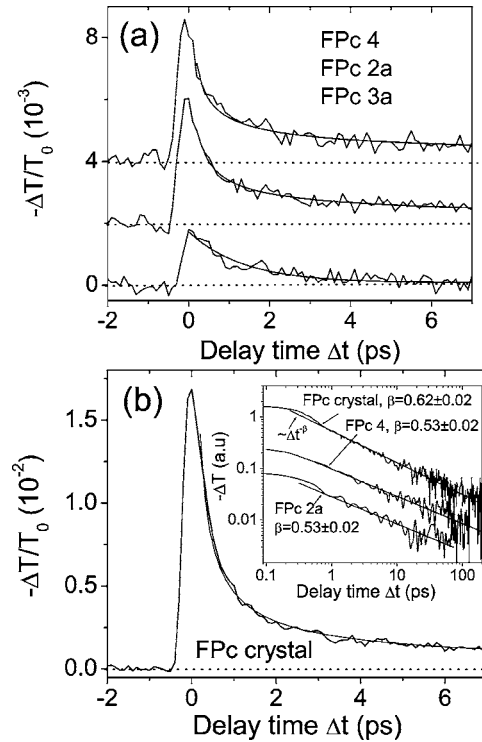


FIG. 9. Differential transmission ( $-\Delta T/T_0$ ) as a function of pump-probe delay time ( $\Delta t$ ) observed in (a) films FPC 2*a* (evaporated at  $T_s=85^\circ\text{C}$ , on mica), 3*a* (evaporated at  $T_s=25^\circ\text{C}$ , on mica), and 4 (solution grown at  $T_s=25^\circ\text{C}$ , on glass), and (b) FPC single-crystal sample. A single exponential fit ( $\exp[-\Delta t/\tau]$ ,  $\tau=1.35$  ps) to the data obtained in film FPC 3*a* as well as power-law fits ( $\Delta t^{-\beta}$ ) obtained in (a) films FPC 2*a* and FPC 4, and (b) a FPC single-crystal sample are also shown. Transients are offset along the  $y$  axis in (a) for clarity. The inset shows a log-log plot of the differential transmission data (offset along the  $y$  axis for clarity) obtained in the films FPC 2*a* and FPC 4 and a FPC single-crystal sample. Power-law fits and corresponding values for  $\beta$  are also included.

$T_s=25^\circ\text{C}$ ) and a value twice as large of  $\sim 0.06\text{ cm}^2/\text{V s}$  in the films FPC 2*a* and FPC 2*b* (prepared by evaporation at  $T_s=85^\circ\text{C}$ ) as well as FPC 4 (solution grown) (Table II). In fact, the  $\mu\eta$  product of  $0.06\text{ cm}^2/\text{V s}$  obtained in the films FPC 2*a*, FPC 2*b*, and FPC 4 is about 30%–40% of that observed in FPC single-crystal samples at room temperature of  $0.15$ – $0.2\text{ cm}^2/\text{V s}$ , depending on the sample.<sup>28,31</sup> Among all the FPC films studied, the smallest value obtained for the  $\mu\eta$  product was  $\leq 0.01\text{ cm}^2/\text{V s}$  in the “amorphous” films FPC 1 (*a*, *a'*, and *b*), and the decay dynamics in these films could not be analyzed due to an insufficient signal-to-noise ratio. Among the samples FPC 2 (*a* and *b*), FPC 3 (*a*, *a'*, and *b*), and FPC 4, the films FPC 3 (*a*, *a'*, and *b*) exhibited the fastest decay dynamics described by a single-exponential ( $\exp[-\Delta t/\tau]$ ) with  $\tau\sim 0.6$ – $1.4$  ps [Fig. 9(a) and Table II]. In contrast, in films FPC 2*a*, FPC 2*b*, and FPC 4, the decay dynamics persisted over at least  $\sim 100$  ps and could be fitted by the power-law function  $\Delta t^{-\beta}$  with  $\beta=0.53$  [inset of Fig. 9(b)]. This behavior is similar to that obtained in FPC single crystals, as shown in Fig. 9(b), in which the decay dynamics are characterized by a power-law function with  $\beta\sim 0.5$ – $0.7$  [ $\beta=0.62$  is shown in the inset of Fig. 9(b)].<sup>28,31,35</sup>

The difference in the decay dynamics observed in the FPC films can be related to their structure. The SEM images of the films FPC 2*b* and FPC 3*b* are shown in Figs. 10(a) and



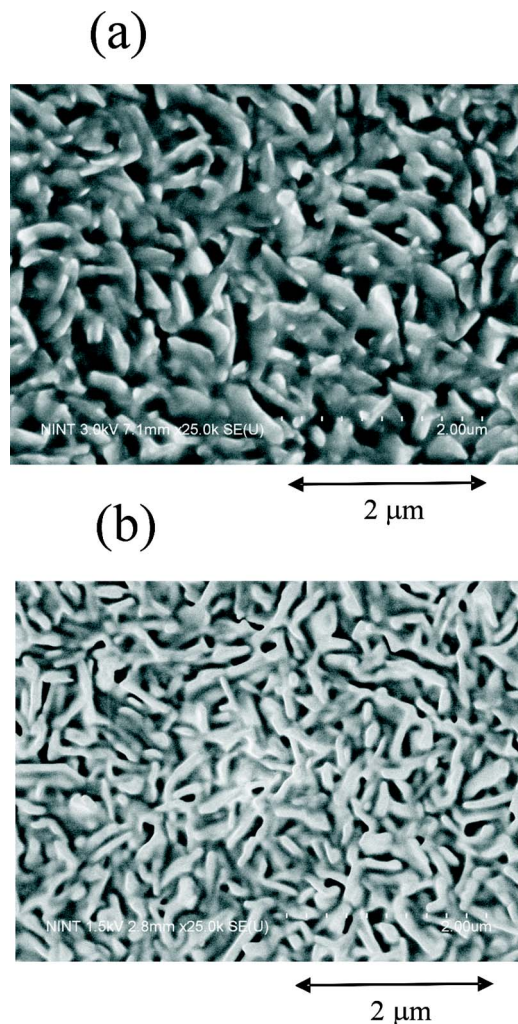


FIG. 10. Scanning electron microscopy images of the films (a) FPC 2*b* (evaporated at  $T_s=85^\circ\text{C}$ , on glass) at an accelerating voltage of 3 kV, and (b) FPC 3*b* (evaporated at  $T_s=25^\circ\text{C}$ , on glass) at an accelerating voltage of 1.5 kV.

10(b), respectively. While the film FPC 3*b* appears to contain small randomly interconnected domains, the film FPC 2*b* consists of larger crystallites [see also Fig. 7(b)]. As a result, in the film FPC 3*b* (or morphologically similar FPC 3*a*), a fast single-exponential decay of the transient photoconductivity is observed [Fig. 9(a)] as the charge carriers are trapped on the grain boundaries and/or defects within several picoseconds after photoexcitation. In contrast, the larger crystallites of film FPC 2*b* (or FPC 2*a*) support longer charge-carrier lifetimes, resulting in power-law decays of the transient photoconductivity similar to the single-crystal results over at least 100 ps [inset of Fig. 9(b)].

#### IV. DISCUSSION

It is well known that optical-absorption spectra of organic semiconductor thin films depend on the structure and morphology of the film,<sup>13,14,17,47,54</sup> which is clearly demonstrated in the case of our FPC films (Fig. 6). In particular, compared to the spectra of amorphous films and solution, those of polycrystalline films exhibit significant redshift, broader bands, and stronger coupling between the electronic

and vibrational transitions. Optical-absorption spectra of Pc and FPC films reflect the difference in the molecular packing of Pc and FPC molecules in a unit cell,<sup>33</sup> which is also a reason for dramatically different temperature dependences of Pc and FPC spectra (Figs. 3 and 8).

Regardless of morphology, all Pc and FPC films studied exhibited subpicosecond charge-carrier photogeneration (Figs. 4 and 9). Such ultrafast photoresponse of our films allowed us to observe terahertz generation in a photoconductive switch geometry (Fig. 5). As we have previously reported, the photogeneration efficiency for mobile charge carriers ( $\eta$ ) over subpicosecond time scales in Pc and FPC thin films and FPC single crystals is wavelength independent and is not thermally activated.<sup>31,32</sup> These experimental results are inconsistent with exciton dissociation mechanisms<sup>2,55</sup> and suggest that mobile carriers, not just excitons, are a primary photoexcitation.<sup>7,28,29,56</sup> Although in our experiments we could not detect the presence of excitons in Pc and FPC samples, most likely due to a small exciton polarizability at terahertz frequencies, numerous studies have shown that upon photoexcitation of polyacenes a large population of excitons is formed,<sup>2,6,57</sup> which contributes to photoconductivity at longer time scales, including dc photoconductivity.<sup>46</sup> Therefore, the photogeneration efficiency  $\eta$  for the primary photoexcitation of mobile charge carriers is most likely less than unity, since excitons may also be formed in the initial photoexcitation process.<sup>30,57,58</sup>

Charge transport properties of pentacene derivatives have been extensively studied mostly in the field-effect, space-charge-limited current, and two- or four-point contact configurations.<sup>8–10,19,52,59</sup> Despite numerous efforts to improve the quality of single crystals and thin films (such as growth conditions, purification, substrate pretreatment, etc.), the charge-carrier mobility obtained from most of these measurements is thermally activated (i.e., mobility increases as the temperature increases). As previously shown,<sup>28,29,31</sup> however, the mobility extracted from the peak amplitude of the terahertz differential transmission  $[-\Delta T(0)/T_0]$  measured in Pc and FPC thin films prepared without any purification or pretreatment increases as the temperature decreases in a wide temperature range from 300 down to 5 K, a signature of bandlike transport. The possible physical mechanism of the charge transport on picosecond time scales in these materials is consistent with the nearly small molecular polaron (MP) model,<sup>6</sup> which describes the propagation of the MP (forming as a result of interaction of a charge carrier with intramolecular vibrations and infrared-active modes of the nearest-neighbor molecules) from site to site by “stepping via tunneling,” while retaining bandlike features, such as mobility increasing as the temperature decreases. The time scales on which the MP transport (rather than the thermally activated transport) can be observed in polyacene thin films depend on the structure and morphology of the film. Indeed, in FPC films with smaller crystalline domains [e.g., FPC 3*b*, Fig. 10(b)] the observation of MP transport at times longer than several picoseconds after the photoexcitation is impaired due to deep-level trapping at the grain boundaries. In contrast, the films with larger crystallites such as FPC 2*b* [Fig. 10(a)] and FPC 4 exhibit long power-law decay dynamics over time

scales at least up to  $\sim 100$  ps, similar to those observed in FPc single crystals. Such differences in the decay dynamics of the transient photoconductivity depending on the structure and morphology of the films suggest that our measurements may be able to trace directly the time scale for crossover from the bandlike to thermally activated charge transport. For example, in thin FPc films with smaller domains, the charge carriers are trapped in deep-level traps within a few picoseconds, after which a trap-dominated (and thus, thermally activated) transport could be expected, while in considerably better films and single crystals, the bandlike charge transport extends over time scales of at least several hundred picoseconds.

Although one could expect a direct link between the film crystallite size and the decay dynamics of the transient photoconductivity in films made of the same material (e.g., FPc), it is not clear yet how to unambiguously interpret and compare the decay dynamics observed in films made of different materials such as, for example, FPc and Pc. Although the grain sizes in the best FPc and Pc films were comparable, fast single or biexponential decay dynamics (i.e.,  $\exp[-\Delta t/\tau]$  with  $\tau \sim 0.7-1$  ps or  $A \exp[-\Delta t/\tau_1] + B \exp[-\Delta t/\tau_2]$  with  $\tau_1 \sim 0.6-1.2$  ps,  $\tau_2 \sim 5-16$  ps, and  $A/(A+B) \sim 0.8-0.9$ ) were obtained in Pc films at room temperature (Ref. 31 and Fig. 4), in contrast with longer power-law decays [ $\sim (\Delta t)^{-\beta}$ ,  $\beta \sim 0.53$ ] observed in the best FPc films (e.g., FPc 2*b* and FPc 4 in Fig. 9). In order to clarify whether this difference is related to a difference in molecular packing, structural or chemical traps, or quality of domain boundaries, further studies are needed.

It is interesting to note that the optical-pump-terahertz-probe studies by Thorsmølle *et al.*<sup>29</sup> on Pc single crystals revealed photocarrier decay dynamics with fast ( $\sim 0.8$  ps) and slow ( $\sim 4$  ps) components, similar to what was observed here for polycrystalline Pc thin films. However, the room-temperature  $\mu\eta$  product measured by Thorsmølle *et al.*<sup>29</sup> for Pc single crystals was approximately  $0.2 \text{ cm}^2/\text{V s}$ , which is higher than the values measured here of  $0.02-0.04 \text{ cm}^2/\text{V s}$  for polycrystalline Pc thin-film samples. The similar decay dynamics but lower  $\mu\eta$  product for the Pc thin films compared to single crystals would suggest that the photogeneration efficiency  $\eta$  in the Pc thin-film samples was lower than that in Pc single crystals. This may be due to fast trapping or recombination of mobile carriers generated at (or near) the grain boundaries in the polycrystalline Pc thin films over time scales shorter than the 0.4-ps time resolution of our setup. The number of photocarriers that remained mobile within the grains for times longer than 0.4 ps would then determine the magnitude of the observed photoconductive transient (i.e.,  $|\Delta T(0)/T_0|$ ), which is used to obtain the  $\mu\eta$  product from Eq. (1). The average carrier density seen by the terahertz probe pulse, which has a spot size ( $\sim 1$  mm) much larger than the typical grain size in the polycrystalline films, would be much lower in the thin-film samples compared to bulk single crystals. This would result in lower  $\mu\eta$  products for the thin-film samples.

The  $\mu\eta$  product calculated from the peak values of the transient photoconductivity measured in our FPc thin-film samples ranged from less than  $0.01 \text{ cm}^2/\text{V s}$  to as high as

$0.06 \text{ cm}^2/\text{V s}$ , depending on the film (Secs. III A 2 a and III B 2). The films FPc 2 (*a* and *b*) prepared by thermal evaporation on a heated substrate ( $T_s = 85^\circ \text{C}$ ) and the FPc 4 film grown from solution exhibited the highest  $\mu\eta$  values of all the films studied of  $\sim 0.06 \text{ cm}^2/\text{V s}$ . Considering that this value is only a factor of  $\sim 3$  below that obtained in FPc single-crystal samples ( $\mu\eta \sim 0.15-0.2 \text{ cm}^2/\text{V s}$  at room temperature), we conclude that these preparation methods yield polycrystalline films with the best transient photoconductive properties. Although in our measurements we cannot separate the charge-carrier mobility  $\mu$  and photogeneration efficiency  $\eta$ , the obtained values of  $\mu\eta$  provide an estimate of the lower limit of the mobility if we assume  $\eta = 1$  in our samples. However, as mentioned above,  $\eta < 1$  due to a significant population of excitons that do not contribute to our subpicosecond photoconductivity signal as well as initial carrier trapping and recombination that occurs within 400 fs after excitation, not resolved in our experiments.<sup>31</sup> The charge-carrier mobilities, therefore, are most likely higher than those listed for  $\mu\eta$  in Table II. The power-law decays seen in the transient photoconductive response of films FPc 2*a* and FPc 4 have  $\beta$  values similar to those observed in FPc single crystals [inset of Fig. 9(b)], but the peak values of the photoconductive response are very different. The similarity in decay dynamics compared to single crystals implies that we are probing intrinsic carrier dynamics within the grains of the best polycrystalline FPc films. However, as discussed above for the Pc films, the magnitude of the photoconductive transient is lower in the FPc thin-film samples due to recombination or trapping of photogenerated charge carriers at (or near) the grain boundaries at short time scales ( $< 0.4$  ps). Therefore, a peak photoconductive response for the best FPc thin films that is a factor of  $\sim 3$  lower than that obtained in FPc single crystals would suggest that, out of all the primary charge-carrier photoexcitations initially generated by the pump pulse in the FPc films, only about 30% of those primary carriers remain mobile in the sample after 0.4 ps and are located within the crystalline grains (if we assume that the carrier mobility within each grain is the same as that in the bulk single-crystal samples). The terahertz pulse then probes the charge transport within the crystalline grains, which results not only in similar decay dynamics to that seen in single crystals but also the observation of bandlike transport, as previously reported in Pc and FPc films.<sup>31</sup> If we also consider a further reduction in  $\eta$  due to the generation of primary excitons, then we expect the carrier mobility  $\mu$  in our best FPc films to be much higher than  $0.06 \text{ cm}^2/\text{V s}$ . For example, if we assume that  $\sim 10\%$  of all the primary photoexcitations are mobile charge carriers [as reported for poly[2-methoxy-5-(2'-ethyl-hexyloxy)-1,4-phenylene vinylene] (MEH-PPV) in Ref. 58], and that  $\sim 30\%$  of those carriers survive beyond 0.4 ps within each grain, then the carrier mobility in the grains would actually be  $\sim 2 \text{ cm}^2/\text{V s}$ . Nevertheless, mobility values larger than  $0.06 \text{ cm}^2/\text{V s}$  in our best FPc films are consistent with those measured by Sheraw *et al.*<sup>19</sup> of  $0.05-0.4 \text{ cm}^2/\text{V s}$  using field-effect transistor (FET) devices on FPc (TIPS) thin films evaporated on pre-treated substrates.

## V. CONCLUSIONS

In summary, we presented the optical and transient photoconductive properties of a variety of pentacene and functionalized pentacene thin films. Optical-absorption spectra depend on the temperature as well as on the structure and morphology of the films. In all samples, subpicosecond photogeneration of mobile charge carriers was observed. The lower limits of charge-carrier mobility calculated from the amplitude of the transient photoconductivity in the *a-b* plane of the crystallites were  $\sim 0.04 \text{ cm}^2/\text{V s}$  and  $\sim 0.06 \text{ cm}^2/\text{V s}$  in the best pentacene and functionalized pentacene films, respectively. Preparation methods utilizing either thermal evaporation and a heated substrate ( $T_s = 85 \text{ }^\circ\text{C}$ ) or growth from solution yielded the best functionalized pentacene films. These films exhibited photoconductivity transients reaching 30%–40% of those in functionalized pentacene single crystals as well as similar power-law decay dynamics as single-crystal samples over at least  $\sim 100 \text{ ps}$ . In pentacene films and functionalized pentacene films with a small grain size, smaller photoconductivity transients as well as single or biexponential decay dynamics were observed.

## ACKNOWLEDGMENTS

The authors are grateful to Steven Launspach of the National Institute for Nanotechnology (Edmonton, Canada) for technical assistance with the AFM and SEM characterizations. We also thank Hue Nguyen of the Nanofabrication Center for the film thickness measurements and Jianbo Gao for gold deposition. This work was supported by NSERC, CFI, CIPI, iCORE, and ONR. One of the authors (O.O.) acknowledges the Killam Trust for a Killam Memorial Postdoctoral Fellowship.

<sup>1</sup>F. Gutmann and L. E. Lyons, *Organic Semiconductors* (Wiley, New York, 1967).

<sup>2</sup>M. Pope and C. E. Swenberg, *Electronic Processes in Organic Crystals and Polymers*, 2nd ed. (Oxford University Press, New York, 1999).

<sup>3</sup>S. R. Forrest, *Nature* (London) **428**, 911 (2004); T. W. Kelley, P. F. Baude, C. Gerlach, D. E. Ender, D. Muires, M. A. Haase, D. E. Vögel, and S. D. Theiss, *Chem. Mater.* **16**, 4413 (2004).

<sup>4</sup>C. D. Dimitrakopoulos and P. R. L. Malenfant, *Adv. Mater.* (Weinheim, Ger.) **14**, 99 (2002).

<sup>5</sup>N. S. Sariciftci, *Primary Photoexcitations in Conjugated Polymers: Molecular Exciton versus Semiconductor Band Model* (World Scientific, Singapore, 1997); M. L. Tiago, J. E. Northrup, and S. G. Louie, *Phys. Rev. B* **67**, 115212 (2003); R. C. Haddon, X. Chi, M. E. Itkis, J. E. Anthony, D. L. Eaton, T. Siegrist, C. C. Mattheus, and T. T. M. Palstra, *J. Phys. Chem. B* **106**, 8288 (2002); K. Hannewald and P. A. Bobbert, *Appl. Phys. Lett.* **85**, 1535 (2004); V. Gulbinas, Yu. Zaushitsyn, H. Bässler, A. Yartsev, and V. Sundström, *Phys. Rev. B* **70**, 035215 (2004).

<sup>6</sup>E. A. Silinsh and V. Čápec, *Organic Molecular Crystals: Interaction, Localization and Transport Phenomena* (American Institute of Physics, New York, 1994).

<sup>7</sup>P. B. Miranda, D. Moses, and A. J. Heeger, *Phys. Rev. B* **64**, 081202(R) (2001).

<sup>8</sup>O. D. Jurchescu, J. Baas, and T. T. M. Palstra, *Appl. Phys. Lett.* **84**, 3061 (2004).

<sup>9</sup>S. F. Nelson, Y. Y. Lin, D. J. Gundlach, and T. N. Jackson, *Appl. Phys. Lett.* **72**, 1854 (1998).

<sup>10</sup>D. Knipp, R. A. Street, and A. R. Völkel, *Appl. Phys. Lett.* **82**, 3907 (2003).

<sup>11</sup>M. M. Ling and Z. Bao, *Chem. Mater.* **16**, 4824 (2004).

<sup>12</sup>J. C. Scott, *J. Vac. Sci. Technol. A* **21**, 521 (2003); P. V. Pesavento, R. J. Chesterfield, C. R. Newman, and C. D. Frisbie, *J. Appl. Phys.* **96**, 7312 (2004).

<sup>13</sup>K. O. Lee and T. T. Gan, *Chem. Phys. Lett.* **51**, 120 (1977).

<sup>14</sup>R. Hesse, W. Hofberger, and H. Bässler, *Chem. Phys.* **49**, 201 (1980).

<sup>15</sup>R. Elermann, G. M. Parkinson, H. Bässler, and J. M. Thomas, *J. Phys. Chem.* **87**, 544 (1983).

<sup>16</sup>C. D. Dimitrakopoulos, A. R. Brown, and A. Pomp, *J. Appl. Phys.* **80**, 2501 (1996); W. Takashima, S. S. Pandey, T. Endo, M. Rikukawa, N. Tanigaki, Y. Yoshida, K. Yase, and K. Kaneto, *Thin Solid Films* **393**, 334 (2001); A. J. Mozer, P. Denk, M. C. Scharber, H. Neugebauer, N. S. Sariciftci, P. Wagner, L. Lutsen, and D. Vanderzande, *J. Phys. Chem. B* **108**, 5235 (2004); H. J. Snaith and R. H. Friend, *Thin Solid Films* **451–452**, 567 (2004); G. Witte and C. Woll, *J. Mater. Res.* **19**, 1889 (2004).

<sup>17</sup>T. Jentzsch, H. J. Juepner, K. W. Brzezinka, and A. Lau, *Thin Solid Films* **315**, 273 (1998).

<sup>18</sup>M. Shtein, J. Mapel, J. B. Benziger, and S. R. Forrest, *Appl. Phys. Lett.* **81**, 268 (2002); K. Shankar and T. N. Jackson, *J. Mater. Res.* **19**, 2003 (2004).

<sup>19</sup>C. D. Sheraw, T. N. Jackson, D. L. Eaton, and J. E. Anthony, *Adv. Mater.* (Weinheim, Ger.) **15**, 2009 (2003).

<sup>20</sup>P. C. Chang, J. Lee, D. Huang, V. Subramanian, A. R. Murphy, and J. M. J. Frechet, *Chem. Mater.* **16**, 4783 (2004).

<sup>21</sup>C. A. Schmuttenmaer, *Chem. Rev.* (Washington, D.C.) **104**, 1759 (2004).

<sup>22</sup>M. C. Nuss and J. Orenstein, in *Topics in Applied Physics*, edited by G. Gruner (Springer, Berlin, 1998), Vol. 74; D. Mittleman, *Sensing with THz radiation* (Springer, New York, 2003).

<sup>23</sup>M. C. Beard, G. M. Turner, and C. A. Schmuttenmaer, *Phys. Rev. B* **62**, 15764 (2000); P. U. Jepsen, W. Schairer, I. H. Libon, U. Lemmer, N. E. Hecker, M. Birkholz, K. Lips, and M. Schall, *Appl. Phys. Lett.* **79**, 1291 (2001).

<sup>24</sup>K. P. H. Lui and F. A. Hegmann, *Appl. Phys. Lett.* **78**, 3478 (2001).

<sup>25</sup>M. C. Beard, G. M. Turner, and C. A. Schmuttenmaer, *Nano Lett.* **2**, 983 (2002).

<sup>26</sup>E. Knoesel, M. Bonn, J. Shan, F. Wang, and T. F. Heinz, *J. Chem. Phys.* **121**, 394 (2004).

<sup>27</sup>J. Shan, F. Wang, E. Knoesel, M. Bonn, and T. F. Heinz, *Phys. Rev. Lett.* **90**, 247401 (2003).

<sup>28</sup>F. A. Hegmann, R. R. Tykwinski, K. P. H. Lui, J. E. Bullock, and J. E. Anthony, *Phys. Rev. Lett.* **89**, 227403 (2002).

<sup>29</sup>V. K. Thorsmølle, R. D. Averitt, X. Chi, D. J. Hilton, D. L. Smith, A. P. Ramirez, and A. J. Taylor, *Appl. Phys. Lett.* **84**, 891 (2004).

<sup>30</sup>E. Hendry, J. M. Schins, L. P. Candias, L. D. A. Siebbeles, and M. Bonn, *Phys. Rev. Lett.* **92**, 196601 (2004).

<sup>31</sup>O. Ostroverkhova, D. G. Cooke, S. Shcherbyna, R. F. Egerton, F. A. Hegmann, R. R. Tykwinski, and J. E. Anthony, *Phys. Rev. B* **71**, 035204 (2005).

<sup>32</sup>O. Ostroverkhova, S. Shcherbyna, D. G. Cooke, R. Egerton, R. R. Tykwinski, J. E. Anthony, and F. A. Hegmann, *Proc. SPIE* **5517**, 163 (2004).

<sup>33</sup>J. E. Anthony, J. S. Brooks, D. L. Eaton, and S. R. Parkin, *J. Am. Chem. Soc.* **123**, 9482 (2001).

<sup>34</sup>J. E. Anthony, D. L. Eaton, and S. R. Parkin, *Org. Lett.* **4**, 15 (2002).

<sup>35</sup>F. A. Hegmann, O. Ostroverkhova, J. Gao, L. Barker, R. R. Tykwinski, J. E. Bullock, and J. E. Anthony, *Proc. SPIE* **5352**, 196 (2004).

<sup>36</sup>M. A. Wolak, B. B. Jang, L. C. Palilis, and Z. H. Kafafi, *J. Phys. Chem. B* **108**, 5492 (2004); K. Sakai, S. Ohshima, A. Uchida, I. Oonishi, S. Fujisawa, and U. Nagashima, *J. Phys. Chem.* **99**, 5909 (1995).

<sup>37</sup>A. Maliakal, K. Raghavachari, H. E. Katz, E. Chandross, and T. Siegrist, *Chem. Mater.* **16**, 4980 (2004).

<sup>38</sup>F. A. Hegmann and K. P. H. Lui, *Proc. SPIE* **4643**, 31 (2002).

<sup>39</sup>E. Hendry, M. Koeberg, J. M. Schins, H. K. Nienhuys, V. Sundström, L. D. A. Siebbeles, and M. Bonn, *Phys. Rev. B* **71**, 125201 (2005).

<sup>40</sup>R. Ruiz *et al.*, *Chem. Mater.* **16**, 4497 (2004).

<sup>41</sup>D. J. Gundlach, T. N. Jackson, D. G. Schlom, and S. F. Nelson, *Appl. Phys. Lett.* **74**, 3302 (1999).

<sup>42</sup>M. Brinkmann *et al.*, *J. Phys. Chem. B* **107**, 10531 (2003).

<sup>43</sup>J. Lee, S. S. Kim, K. Kim, J. H. Kim, and S. Im, *Appl. Phys. Lett.* **84**, 1701 (2004).

<sup>44</sup>H. C. Wolf, in *Solid State Physics* edited by F. Seitz and D. Turnbull (Academic, New York, 1959).

<sup>45</sup>A. S. Davydov, *Theory of Molecular Excitons* (Plenum, New York, 1971).

<sup>46</sup>D. V. Lang, X. Chi, T. Siegrist, A. M. Sergent, and A. P. Ramirez, *Phys. Rev. Lett.* **93**, 086802 (2004).

<sup>47</sup>R. Jankowiak, K. D. Rockwitz, and H. Bässler, *J. Phys. Chem.* **87**, 552 (1983).

<sup>48</sup>B. B. Hu, A. S. Weling, D. H. Auston, A. V. Kuznetsov, and C. J. Stanton, *Phys. Rev. B* **49**, 2234 (1994); P. U. Jepsen, R. H. Jacobsen, and S. R.

- Keiding, J. Opt. Soc. Am. B **13**, 2424 (1996); H. Němec, A. Pashkin, P. Kužel, M. Khazan, S. Schnull, and I. Wilke, J. Appl. Phys. **90**, 1303 (2001).
- <sup>49</sup>X. C. Zhang, X. F. Ma, Y. Jin, T. M. Lu, E. P. Boden, P. D. Phelps, K. R. Stewart, and C. P. Yakymyshyn, Appl. Phys. Lett. **61**, 3080 (1992); H. Hashimoto, H. Takahashi, T. Yamada, K. Kuroyanagi, and T. Kobayashi, J. Phys.: Condens. Matter **13**, L529 (2001); J. J. Carey, R. T. Bailey, D. Pugh, J. N. Sherwood, F. R. Cruickshank, and K. Wynne, Appl. Phys. Lett. **81**, 4335 (2002); L. M. Hayden, A. M. Sinyukov, M. R. Leahy, J. French, P. Lindahl, W. N. Herman, R. J. Twieg, and M. He, J. Polym. Sci., Part B: Polym. Phys. **41**, 2492 (2003); T. Taniuchi, S. Okada, and H. Nakanishi, J. Appl. Phys. **95**, 5984 (2004); G. M. Mikheev, R. G. Zonov, A. N. Obraztsov and Yu. P. Svirko, Appl. Phys. Lett. **84**, 4854 (2004).
- <sup>50</sup>C. Soci and D. Moses, Synth. Met. **139**, 815 (2003); E. Hendry, M. Koeberg, J. M. Schins, L. D. A. Siebbeles, and M. Bonn, Phys. Rev. B **70**, 033202 (2004).
- <sup>51</sup>C. Ludwig and J. Kuhl, Appl. Phys. Lett. **69**, 1194 (1996).
- <sup>52</sup>T. Tokumoto, J. S. Brooks, R. Clinite, X. Wei, J. E. Anthony, D. L. Eaton, and S. R. Parkin, J. Appl. Phys. **92**, 5208 (2002).
- <sup>53</sup>K. Pichler, D. A. Halliday, D. D. C. Bradley, P. L. Burn, R. H. Friend, and A. B. Holmes, J. Phys.: Condens. Matter **5**, 7155 (1993); S. H. Lim, T. G. Bjorklund, and C. J. Bardeen, Chem. Phys. Lett. **342**, 555 (2001).
- <sup>54</sup>T. W. Hagler, K. Pakbaz, K. F. Voss, and A. J. Heeger, Phys. Rev. B **44**, 8652 (1991); T. Onodera, H. Kasai, S. Okada, H. Oikawa, K. Mizuno, M. Fujitsuka, O. Ito, and H. Nakanishi, Opt. Mater. **21**, 595 (2002).
- <sup>55</sup>V. Arkhipov, E. V. Emelianova, S. Barth, and H. Bässler, Phys. Rev. B **61**, 8207 (2000).
- <sup>56</sup>D. Moses, J. Wang, G. Yu, and A. J. Heeger, Phys. Rev. Lett. **80**, 2685 (1998).
- <sup>57</sup>C. Jundt, G. Klein, B. Sipp, J. Le Moigne, M. Joucla, and A. A. Villaeys, Chem. Phys. Lett. **241**, 84 (1995).
- <sup>58</sup>D. Moses, A. Dogariu, and A. J. Heeger, Phys. Rev. B **61**, 9373 (2000).
- <sup>59</sup>J. Takeya, C. Goldmann, S. Haas, K. P. Pernstich, B. Ketterer, and B. Batlogg, J. Appl. Phys. **94**, 5800 (2003); J. S. Brooks, D. L. Eaton, J. E. Anthony, S. R. Parkin, J. W. Brill, and Y. Sushko, Curr. Appl. Phys. **1**, 301 (2001); V. Y. Butko, X. Chi, D. V. Lang, and A. P. Ramirez, Appl. Phys. Lett. **83**, 4773 (2003); J. S. Brooks, T. Tokumoto, E. S. Choi, D. Graf, N. Biskup, D. L. Eaton, J. E. Anthony, and S. A. Odom, J. Appl. Phys. **96**, 3312 (2004).